Atomic-Scale Defects Might Determine the Second Harmonic Generation from Plasmonic Graphene Nanostructures

François Aguillon, Andrei G Borisov

Atomic-Scale Defects Might Determine the Second Harmonic Generation from Plasmonic Graphene Nanostructures

François Aguillon and Andrei G. Borisov*

Institut des Sciences Moléculaires d'Orsay, UMR 8214, CNRS, Université Paris-Saclay, Bâtiment 520, 91405 Orsay Cedex, France

E-mail: andrei.borissov@u-psud.fr

Phone: +33 (0)1 69157697

Abstract

In this work we theoretically investigate the impact of the atomic scale lattice imperfections of graphene nanoflakes on their nonlinear response enhanced by the resonance between an incident electromagnetic field and localized plasmon. As a case study we address the second harmonic generation from graphene plasmonic nanoantennas of different symmetry with missing carbon atom vacancy defects in the honeycomb lattice. Using the many-body time-dependent density matrix approach we find that one defect in the nanoflake comprising over five thousand carbon atoms can strongly impact the nonlinear hyperpolarizability and override the symmetry constraints. The effect reported here cannot be captured using relaxation time approximation within quatum or classical framework. Results obtained in this work have thus important implications for design of nonlinear graphene devices.

TOC Graphic

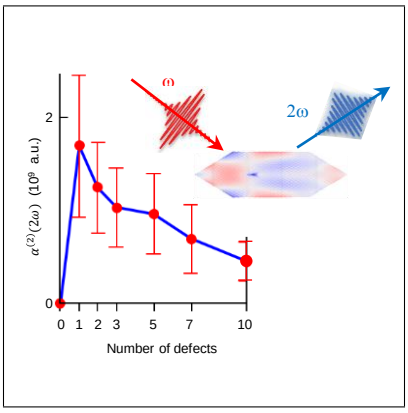

Keywords

plasmonics, single emitter, defects, nanoantennas, graphene

Owing to an electron motion confined to the 2D plane of atoms, and its band-structure characterized by the Dirac cone at the K-point, graphene shows remarkable properties in electron transport, light-matter interaction, and spintronics.[1–8] In particular, multiple experimental and theoretical studies demonstrated that electrical doping allows one to control the linear and nonlinear optical response of graphene nanostructures, which is to large extent enabled by tunability of their collective electronic excitations, 2D graphene plasmons.[6,9–13] The possibility of an active control along with strong nonlinearity makes graphene nanostructures a versatile platforms for linear[6,10,11] and nonlinear[8,14–22] applications in information technologies, wavelength conversion, and sensing among others.

This vast range of possible applications challenges the nanofabrication of graphene nanodevices optimised for the desired linear or nonlinear effects. In this regard, the possible guidance from the theory cannot be overestimated. Since the fabricated nanodevices are unavoidably unperfect on atomic scale (lattice imperfections, substrate effects, adatoms), one naturally questions to which extent the optical response of the realistic nanostructure differs from that of an ideal one. So far, most of the theoretical studies of the linear and nonlinear optical properties of graphene and graphene nanostructures either neglected the lattice imperfections, or accounted for their effect introducing empirical or calculated relaxation time associated with defect scattering,[3,23–25] while considering an ideal graphene lattice (quantum treatments),[12,17,18,26–32] or homogeneous 2D material (classical treatments).[10,11,22,33–39] In this regard, e.g. the Drude dielectric functions[11,17,39–42] contain the relaxation time as a parameter simplifying such an approach.

In this work, using a case study of the second harmonic generation from graphene nanoflakes (GNF's) with lattice defects represented by a carbon atom vacancy, we theoretically demonstrate the "local" effect of the defect scattering which can not be captured by relaxation time approximations described above (see also Ref.[43]). We consider the situation where the incident electromagnetic radiation is at resonance with localized plasmon of the doped GNF. The plasmon excitation is associated with strong enhancement of the

near field and thus of the nonlinear response of the nanostructure.[18,27,29] We compare the nonlinear response of GNF's with geometries chosen such that for an ideal lattice with no defects the second harmonic generation is either (1) efficient, or (2) it is inhibited by the centrosymmetry of the object. Performing quantum-many body calculations we show that single atom vacancy defect concentrations as low as one per several thousands of lattice atoms lift the symmetry constraint and lead to an efficient second harmonic generation. The effective nonlinear second-order susceptibility of the defective GNF is larger than that of such strongly non-linear low-dimensional materials as transition metal dichalogenides.[44] We further demonstrate that irrespective of the nonlinear response for an ideal geometry, nanofaricated GNF's might have similar second harmonic generation efficiency because of the unavoidable defect contribution. Our results thus provide a quantitative insights into the nonlinear optical properties of small graphene nanostructures with lattice defects. The findings reported here are of importance for setting realistic objectives when engineering nonlinear graphene devices.

As representative examples, we study the nonlinear second-order response of the circular (C-type, $N_c = 5520$ carbon atoms), hexagonal (H-type, $N_c = 5514$ carbon atoms), and triangular (T-type, $N_c = 5556$ carbon atoms) GNF's often considered in the context of graphene plasmonics[45] as prototypical nanoantennas allowing enhancement of the incident electromagnetic field and thus of the nonlinear effects.[12,18,29,45–47] The geometry of the nanostructures with carbon atom layer located in the (x, y)-plane is sketched in Figure 1. The H-type and T-type GNF's have armchair edges reducing the localized plasmon decay via adge scattering.[45,48] The charge doping with 100 (C-type), 20 (H-type), and 20 (T-type) electrons added to the neutral nanostructure, and large enough size of the nanostructures (~ 10 nm), allow to obtain well-defined dipolar plasmon resonances in the optical response of the defect-free GNF's[48,49] as shown in Figure 1).

Inline with widely used approaches, the single atom vacancy defect is modeled by removing the carbon atom located at the defect site of the honeycomb lattice of GNF's. While

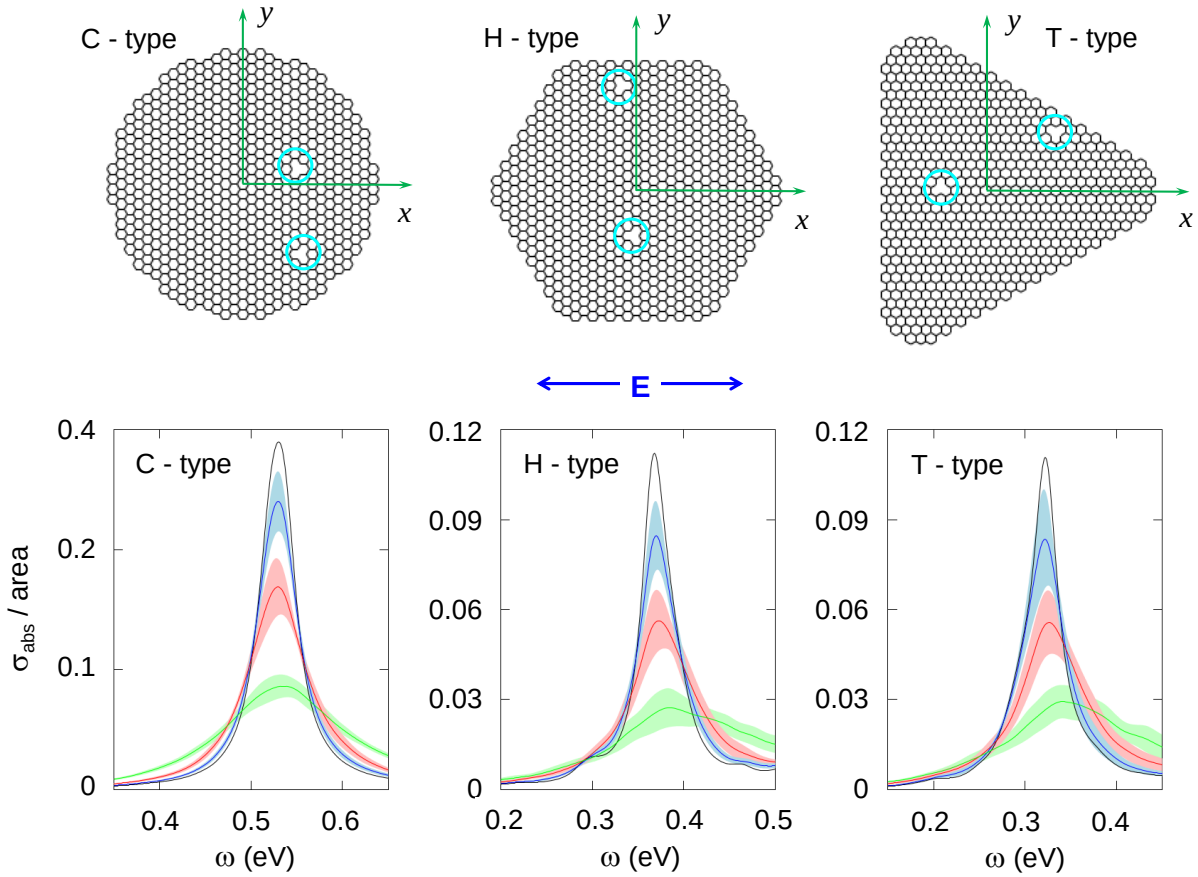

Figure 1: Upper panels: sketch of the circular (C-type), hexagonal (H-type), and triangular (T-type) GNF's studied in this work. Note that for the sake of the visibility of the edges and vacancies, we show GNF's that have spatial dimensions twice smaller than actually studied structures. Two randomly generated missing atom vacancies of the graphene lattice are identified with cyan circles. The blue double arrow indicates the polarization of the incident electromagnetic field. Lower panels: Linear optical response of the doped GNF's. Absorption spectra calculated with TDDM-TB approach are presented as function of the frequency of the incident electromagnetic plane wave. Black line: absorption cross-section, $\sigma_{\rm abs}$ for the defect-free nanoparticles. The colored full lines: absorption cross-sections of GNF's with 1 (blue lines), 3 (red lines), and 10 (green lines) carbon atom vacancy defects at random positions within nanostructure. The results are obtained by an average over 20 random samples. The hatched areas of the corresponding color show the averages cross-section $\pm$ standard deviation.

being an approximation to more complex realistic situations[50–54] this model of the vacancy defects captures the main physics behind the electronic and optical properties of defective graphene.[3,23,25,55–57]

The dynamics of the electron density of GNF's in response to an incident electromagnetic

wave is described within the framework of the time-dependent density matrix approach using the tight-binding description of the electronic structure of graphene (TDDM-TB). The TDDM-TB approach is based on earlier developments[12,18,29,48,49,58,59] and it allows to address large GNFs with well-established collective plasmon modes. The details on the actual implementation of the method are given in Supporting Information (SI). In brief, using the split-operator time-propagation,[60] we solve the Gorini-Kossakowski-Lindblad-Sudarshan (GKLS) quantum master equation for the time-evolution of the density matrix $\hat{\rho}$[61–64] (unless otherwise stated atomic units are used throughout the paper)

$$\frac{\partial \hat{\rho}}{\partial t} = -\frac{i}{\hbar}\left[\hat{H}, \hat{\rho}\right] + \mathfrak{L}_D\left(\hat{\rho}\right). \tag{1}$$

The tight-binding hamiltonian of the system $\hat{H}$ depends on the occupation $\hat{\rho}_{jj}$ of the lattice cites ($j = 1, ..., N_c$) via the non-retarded Coulomb interactions between them. It also comprises the potential owing to the incident x-polarized electromagnetic plane wave with an electric field given by $\mathbf{E}(t) = \mathbf{e}_x E_0 e^{-i\omega t}$, where $\mathbf{e}_x$ is the unit-length vector along x-axis (see Figure 1). The dissipative part of the Lindblad super-operator, is represented in a simple form $\mathfrak{L}_D\left(\hat{\rho}\right) = -\gamma\left(\hat{\rho} - \hat{\rho}^{(0)}\right)$ describing relaxation to the ground-state density matrix $\hat{\rho}^{(0)}$ with a rate γ. Here we use $\gamma = 15$ meV to account for the plasmon decay with excitation of the optical phonons in graphene.[9,11,65,66] The frequency-resolved quantities are obtained from the time-dependent quantities by time-to-frequency Fourier transform.

The plasmon modes of GNF's appear in the calculated linear absorption spectra as absorption resonances allowing analysis of their energies and widths. The second-order hyperpolarizability tensor $\hat{\alpha}^{(2)}(2\omega, \omega, \omega)$ of the 2D nanostructure is obtained from TDDM-TB calculations using the dipole induced at the second-harmonic ($\mathbf{R}_j$ stands for the position vector of the lattice site j)

$$\mathbf{P}(2\omega) = -\sum_{j=1}^{N_c} \mathbf{R}_j \hat{\rho}_{jj}(2\omega), \tag{2}$$

To this end, considering the reflection symmetry with respect to (x, y)-plane, the $\mathbf{P}(2\omega)$ is

represented in the form

$$\mathbf{P}(2\omega) = \sum_{m,n,k} \mathbf{e}_m \alpha^{(2)}_{mnk}(2\omega, \omega, \omega)\ E_n(\omega)\ E_k(\omega). \tag{3}$$

The indexes m, n, k take the values x, y, and $E_n(\omega)$ is the projection of the incident electric field vector $\mathbf{E}(\omega)$ on the corresponding coordinate axis $E_n(\omega) = \mathbf{e}_m \cdot \mathbf{E}(\omega)$.

The efficiency of the second-order nonlinear process is given by the total power $\mathcal{P}$ radiated into the far field at the second harmonic frequency. Considering the x-polarized incident field, it can be expressed as

$$\mathcal{P} = \frac{2}{3} ck^4 \left|\mathbf{P}(2\omega)\right|^2 = \frac{2}{3} ck^4 \left(\left|\alpha^{(2)}_{xxx}(2\omega, \omega, \omega)\right|^2 + \left|\alpha^{(2)}_{yxx}(2\omega, \omega, \omega)\right|^2 \right) E_0^4, \tag{4}$$

where c is the speed of light in vacuum, and the wave vector k is obtained from $2\omega = kc$. Therefore, we will characterize the systems by the parameter

$$\alpha^{(2)}(2\omega) \equiv \sqrt{\left|\alpha^{(2)}_{xxx}(2\omega, \omega, \omega)\right|^2 + \left|\alpha^{(2)}_{yxx}(2\omega, \omega, \omega)\right|^2}, \tag{5}$$

dubbed as second-order hyperpolarizability in the rest of the text.

Prior to the discussion of the second harmonic generation, we describe the major features of the linear response of GNF's considered in this work. The charge doping of GNF's results in well-defined resonances in the absorption spectra shown in Figure 1. Absorption resonances are associated with excitation of localised dipolar plasmon modes[10] (DP) at frequencies $\omega_{DP} = 0.53$ eV (C-type), $\omega_{DP} = 0.37$ eV (H-type), and $\omega_{DP} = 0.32$ eV (T-type). When present, carbon atom vacancies in graphene lattice produce very efficient scattering centers increasing decay and dephasing of the localized plasmons.[11,40,49,66–70] Indeed, even a single vacancy ($\approx 1/5500$ vacancy concentration) notably broadens the plasmon resonance in absorption spectra, while 3 vacancies ($\approx 1/2800$ vacancy concentration) double the plasmon resonance width.

Because of the large incident field enhancement, the nonlinear response of GNF's is strongest when the incident radiation excites dipolar plasmon of GNF's,[18,29] as we further discuss in SI with an example of the H-type nanoflake. Therefore, we focus our work on the resonant situation $\omega = \omega_{DP}$, and we will use the term "resonant" for the corresponding nonlinear response and second-order hyperpolarizability $\alpha^{(2)}(2\omega)$. It is noteworthy that from results shown in Figure 1 one would expect that broadening of the localized plasmons by the vacancy defects leads to smaller 2$^{\text{nd}}$ harmonic generation. As we discuss below, while this effect indeed exists, it is not always the leading consequence of the presence of the lattice imperfections.

We now turn to the second harmonic generation from GNF's with and without carbon atom vacancy defects. An ideal defect-free T-type GNF has been thoroughly studied in the literature.[12,18,29,47] It is characterised by high resonant hyperpolarizability, and permits an efficient second harmonic generation in the far field. In sheer contrast, $\alpha^{(2)}(2\omega) = 0$ for

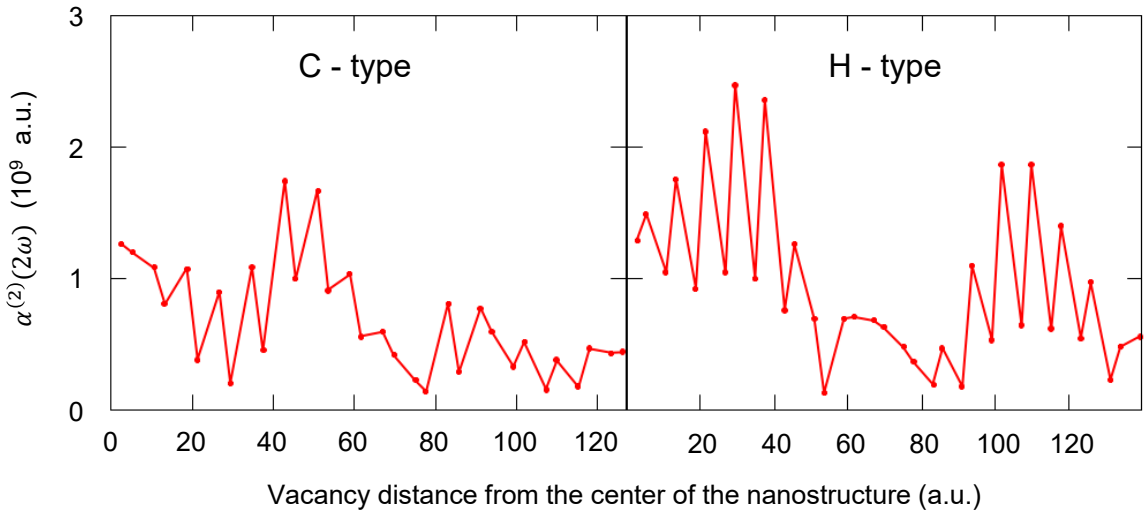

Figure 2: The second-order hyperpolarizability $\alpha^{(2)}(2\omega)$ for the x-polarized electromagnetic plane wave incident at the doped C-type and H-type GNF's (see Figure 1) with single atom vacancy. The incident radiation (fundamental frequency ω) is at resonance with dipolar plasmon of the nanostructure $\omega = \omega_{DP}$. Results are shown in atomic units (10^9 a.u. $= 0.864 \times 10^{-23}$ esu) as function of the vacancy distance from the center of GNF. The vacancy is displaced along the symmetry x-axis ($y = 0$, armchair sequence of the lattice sites).

the defect-free C-type and H-type GNF's i.e. no second harmonic generation is possible in the far field because of the centrosymmetric geometry of these nanoparticles. As soon as the defect breaks the symmetry of the C-type and H-type GNF's, a nonlinear dipole can be induced at the second harmonic frequency with dipolar second harmonic emission into the far field. It is worth noting that the second harmonic is present in the near field of the pristine centrosymmetric nanostructures (see SI), where it results from the high order multipoles.

In Figure 2 we show the resonant hyperpolarizability of the defective C-type and H-type GNF's calculated with TDDM-TB as function of the position of the carbon atom vacancy. The defect is following the armchair sequence along the x-axis ($y = 0$). It follows from our results that even a single carbon atom vacancy present in the nanostructure comprising over 5500 carbon atoms, and displaced from the geometrical center by only one C-C bond length is very efficient in allowing frequency conversion. The resulting hyperpolarizability $\alpha^{(2)}(2\omega)$ is of the same order of magnitude as that of an ideal T-type GNF (7×10^{9} a.u. or 6×10^{-23} esu) which is a prototypical nanoantenna for the second-order nonlinear applications. It is also essentially larger than the nonlinear response of the metal nanostructures of comparable size as analysed in details in Ref.[12] (see also Refs.[5,43]).

The role of the vacancy defect in allowing the resonant second harmonic generation from centrosymmetric GNF's is further analysed in Figure 3. We compare the charge density induced at ω (linear response) and 2ω (nonlinear response) in an ideal and defective H-type GNF. An incident x-polarized electromagnetic plane wave is at resonance with dipolar plasmon of the nanoparticle $\omega = \omega_{DP}$. For an ideal nanostructure without lattice defects, the charge density at the fundamental frequency reflects the dipolar localized plasmon mode excited by an incident field. The induced charge density at the second harmonic shows multipolar character with symmetry such that $\mathbf{P}(2\omega) = 0$. Introducing a single carbon atom vacancy does not affect the dipolar character of the response at the fundamental frequency, albeit the vacancy scatters the optically excited electrons as visible in its vicinity. In sheer

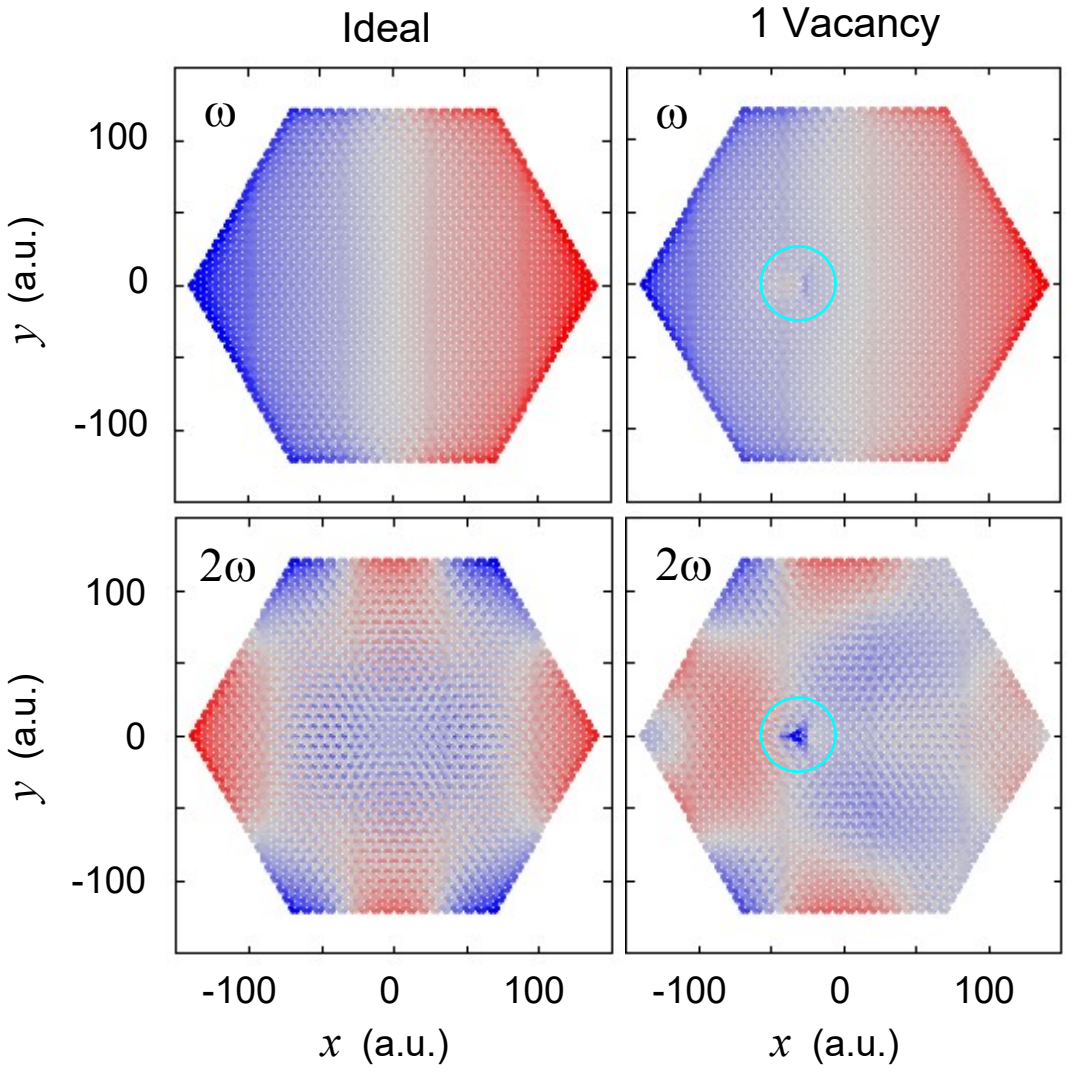

Figure 3: Maps of the charge densities induced at first and second harmonic in the doped H-type GNF. The incident x-polarized electromagnetic plane wave with the field amplitude $E_0 = 5.14 \times 10^{-3}$ V/nm and frequency $\omega = 0.37$ eV is at resonnace with dipolar plasmon of the nanostructure $\omega = \omega_{DP}$. Results are shown as function of x- and y-coordinates defined in Figure 1. Red (blue) color stands for the positive (negative) value of the charge density. The range of the variation of the linear (nonlinear) induced density is $\pm 4 \times 10^{-4}$ a.u. ($\pm 2 \times 10^{-5}$ a.u.). Results for the ideal (no defects) and defective (1 carbon atom vacancy) nanostructures are shown. The blue circle indicates the position of the vacancy defect.

contrast, the vacancy defect leads to the strong change of the induced charge density map at second harmonic frequency. The symmetry break allows for nonlinear dipolar polarisation and therefore second harmonic emission into the far field.

Finally, in Figure 4 we analyse the second harmonic generation from defective GNF's with

different geometries (see Figure 1). Results are shown as function of the number of carbon atom vacancies N_V for the x-polarised incident plane wave with fundamental frequency ω at resonance with dipolar plasmon of the nanostructure $\omega = \omega_{DP}$.

Two distinct behaviours of resonant hyperpolarizability $\alpha^{(2)}(2\omega)$ on N_V are obtained when comparing (i) the C-type, H-type GNF's with geometry silencing the second harmonic generation for an ideal nanoparticle because of the symmetry constraints, and (ii) the T-type GNF allowing an efficient frequency conversion for an ideal nanoparticle. Upon adding defects to an ideal lattice of geometry (i) the second-order hyperpolarizability GNF's first increases, reaches an optimum value at $N_V = 1-3$, and then decreases. This finding indicates a local effect that can not be captured by an effective relaxation time approximation. For the T-type GNF, increasing number of defects continuously reduces the nonlinear response.

The dependence of resonant $\alpha^{(2)}(2\omega)$ on vacancy concentration can be understood as

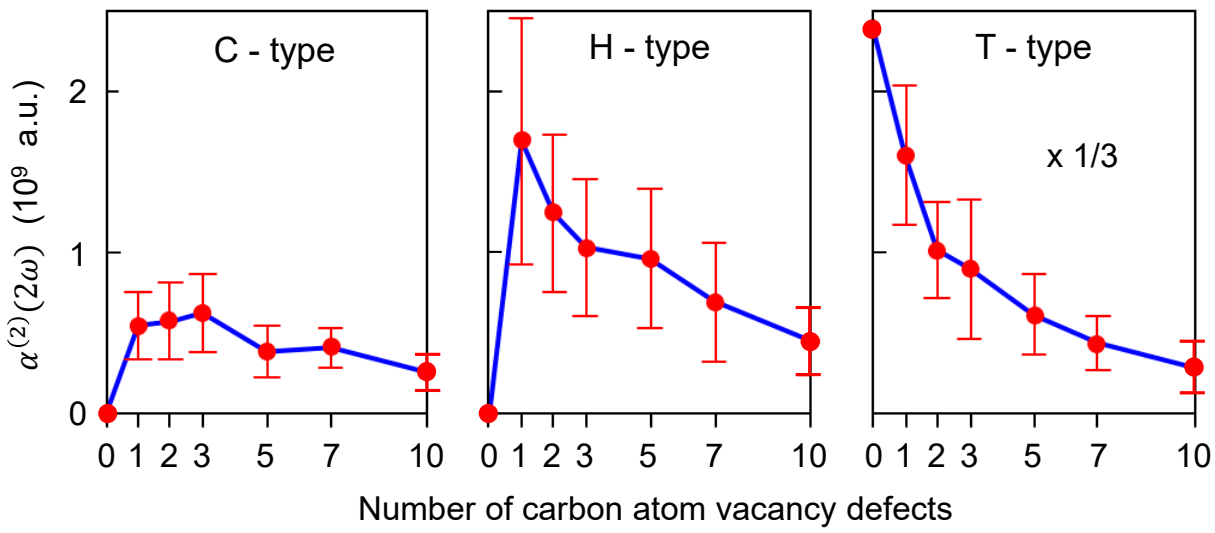

Figure 4: The nonlinear response of the doped defective C-type, H-type, and T-type GNF's calculated at resonance between the incident x-polarized electromagnetic plane wave and dipolar plasmon of the nanoparticle $\omega = \omega_{DP}$. Resonant hyper-polarisability $\alpha^{(2)}(2\omega)$ is shown in atomic units (1×10^9 a.u. $= 0.864 \times 10^{-23}$ esu) as a function of the number of randomly located carbon atom vacancies, N_V. Each data point is obtained by an average over 20 random samples. Each sample corresponds to the N_V vacancies that are randomly generated within GNF. The error bars show the standard deviation. Notice that for the T-type GNF the scaling factor $\times 1/3$ is applied.

follows. For the C-type and H-type GNF's two effects compete. First, the vacancies produce the symmetry break necessary for the second harmonic generation. Second, the broadening of the localized plasmon by the vacancy scattering (see Figure 1), reduces the near fields, and thus the nonlinearity. The interplay between these two effects leads to the existence of the optimal vacancy concentration maximising the second-order nonlinearity. This is in contrast with the T-type GNF which is an efficient frequency convertor for an ideal lattice. In this situation the defects degrade the resonant nonlinear response via the plasmon broadening mechanism and $\alpha^{(2)}(2\omega)$ monotonously decreases with increasing N_V. Noteworthy, we obtain that when ~ 10 vacancies are present in the lattice (0.2% vacancy concentration), GNF's studied here feature similar $\alpha^{(2)}(2\omega)$ irrespective of their geometry. I.e. the vacancy effect determines the second harmonic generation in the system.

Before closing the discussion of the results obtained in this study several comments are in order regarding model representation of the vacancy defect used here, and neglect of the role of the substrate that hosts plasmonic GNF's in practical situations, and can be a source of nonlinear effects.[71,72]

To test the robust character of our results with respect to the model representation of the vacancy defect we calculated resonant $\alpha^{(2)}(2\omega)$ of the defective H-type GNF (i) considering the actual V_1(5-9) mono-vacancy defects[51,52,73] with atomic arrangement determined from *ab initio* calculations in Refs.;[51,74] (ii) considering the defects formed by the substitutional boron and nitrogen atoms.[50,75] These calculations (see details in SI) fully support our findings on the role of the lattice defects in the second harmonic generation from GNF's. It is also worth mentioning that the charged adatom or dipolar admolecule considered earlier in the context of sensing using centrosymmetric GNF's[16] and representing another type of the point defect, lead to comparable nonlinear hyperpolarizability of GNF's.

Furthermore, from the calculated second-order hyperpolarizabilities of GNF's one can obtain their effective surface $\chi_s^{(2)}$ and bulk $\chi_b^{(2)}$ resonant nonlinear susceptibilities. Thus, the single vacancy per 5500 carbon atoms leads to $\chi_s^{(2)} \approx 2.5 \times 10^7 \ \frac{\mathrm{pm}^2}{\mathrm{V}}$ and $\chi_b^{(2)} \approx 7.6 \times 10^4 \ \frac{\mathrm{pm}}{\mathrm{V}}$,

which can be compared with nonlinear second-order response of the 2D layered materials reported in literature. Present results are nearly 10^3 times larger than that of hexagonal boron nitride,[44,76] or of graphene or multilayer graphene triggered by the dc current,[77,78] electrical doping,[79] or symmetry break[79,80] (see also the review by R. Zhou et al[81]). Moreover, the effective $\chi_s^{(2)}$ and $\chi_b^{(2)}$ found here are larger than the second-order susceptibility of such strongly nonlinear materials as transition metal dichalogenides.[44,76,82–84] (See further details in SI.) Therefore, despite the fabrication of plasmonic GNF's implies their deposition on the substrate, such as glass, SiC, or h-BN, the effect of the lattice defects reported here would override[84] the nonlinearity linked with presence of the substrate.

In conclusion, using the many-body time-dependent density matrix approach we addressed the influence of the lattice defects on the second-order nonlinear response of the doped graphene nanostructures. The incident electromagnetic wave is at resonance with localized dipolar plasmon of the nanostructure which increases the nonlinearity. As a case study we considered the single carbon atom vacancy defects within nanoflakes of the geometries prototypical for graphene plasmonics.

As main findings of our work we would like to emphasize the following

- For graphene nanostructures with geometries inhibiting the second harmonic generation in the case of an ideal lattice, a single carbon atom vacancy defect in GNF comprising 5500 carbon atoms lifts this constraint and renders the frequency conversion very efficient. In such a situation, when additionally the incident field is at resonance with dipolar plasmon of the doped GNF, the second harmonic emission into the far field is comparable to that of a triangular graphene nanoantenna considered in the literature as a prototypical system for non-linear applications.

- The resonant second-order hyperpolarizability $\alpha^{(2)}(2\omega)$ calculated for the defective GNF's is essentially larger than that of e.g. metal nanostructures of comparable size. Moreover, the effective second-order nonlinear susceptibility obtained from $\alpha^{(2)}(2\omega)$ for the T-type or defected C-type and H-type GNF's are larger than the data reported for

such strongly nonlinear 2D materials as transition metal dichalogenides.

- For the vacancy concentrations reaching 0.2%, GNF's of different geometries feature similar large $\alpha^{(2)}(2\omega)$. Thus, irrespective of their geometry, defective GNF's are equally efficient for nonlinear applications.

We believe that the quantitative character of our analysis and our qualitative findings are of importance for design and fabrication of graphene nanodevices for nonlinear applications.

Acknowledgement

The authors gratefully acknowledge Dr. Arkady Krasheninnikov and Dr Alberto Zobelli for sharing *ab initio* geometry of the monovacancy V_1(5-9) defect in graphene.

Supporting Information Available

The following files are available free of charge. Supporting information providing details on the

- Time-dependent density matrix method based on the tight-binding description of the electronic structure of graphene.
- The effect of the resonance between the incident electromagnetic radiation and localized dipolar plasmon of graphene nanoflakes on the second harmonic generation.
- The near field induced at the second harmonic.
- The nonlinear response of graphene nanoflakes with $V_1(5-9)$ single atom vacancies and substitutional Nitrogen and Boron atoms.
- The effective surface and volume nonlinear susceptibility of defected graphene nanoflakes and its comparison with measured nonlinear susceptibility of 2D materials.

References

(1) Castro Neto, A. H.; Guinea, F.; Peres, N. M. R.; Novoselov, K. S.; Geim, A. K. The electronic properties of graphene. *Rev. Mod. Phys.* **2009**, *81*, 109–162.

(2) Geim, A. K.; Novoselov, K. S. The rise of graphene. *Nature Materials* **2007**, *6*, 183–191.

(3) Das Sarma, S.; Adam, S.; Hwang, E. H.; Rossi, E. Electronic transport in two-dimensional graphene. *Rev. Mod. Phys.* **2011**, *83*, 407–470.

(4) Han, W.; Kawakami, R. K.; Gmitra, M.; Fabian, J. Graphene spintronics. *Nature Nanotechnology* **2014**, *9*, 794–807.

(5) Hendry, E.; Hale, P. J.; Moger, J.; Savchenko, A. K.; Mikhailov, S. A. Coherent nonlinear optical response of graphene. *Phys. Rev. Lett.* **2010**, *105*, 097401.

(6) Grigorenko, A. N.; Polini, M.; Novoselov, K. S. Graphene plasmonics. *Nature Photonics* **2012**, *6*, 749–758.

(7) Yoshikawa, N.; Tamaya, T.; Tanaka, K. High-harmonic generation in graphene enhanced by elliptically polarized light excitation. *Science* **2017**, *356*, 736–738.

(8) Vermeulen, N. Perspectives on nonlinear optics of graphene: Opportunities and challenges. *APL Photonics* **2022**, *7*, 020901.

(9) Jablan, M.; Buljan, H.; Soljačić, M. Plasmonics in graphene at infrared frequencies. *Phys. Rev. B* **2009**, *80*, 245435.

(10) García de Abajo, F. J. Graphene plasmonics: challenges and opportunities. *ACS Photonics* **2014**, *1*, 135–152.

(11) Low, T.; Avouris, P. Graphene plasmonics for terahertz to mid-infrared applications. *ACS Nano* **2014**, *8*, 1086–1101, PMID: 24484181.

(12) Cox, J. D.; García de Abajo, F. J. Electrically tunable nonlinear plasmonics in graphene nanoislands. *Nature Communications* **2014**, *5*, 5725.

(13) Li, Y.; Li, H.; Wu, S.; Liu, W.-T. Tuning the optical nonlinearity of graphene. *The Journal of Chemical Physics* **2020**, *153*, 080903.

(14) Ooi, K. J. A.; Tan, D. T. H. Nonlinear graphene plasmonics. *Proceedings of the Royal Society A: Mathematical, Physical and Engineering Sciences* **2017**, *473*, 20170433.

(15) Kauranen, M.; Zayats, A. V. Nonlinear plasmonics. *Nature Photonics* **2012**, *6*, 737–748.

(16) Yu, R.; Cox, J. D.; de Abajo, F. J. G. Nonlinear plasmonic sensing with nanographene. *Phys. Rev. Lett.* **2016**, *117*, 123904.

(17) Jablan, M.; Chang, D. E. Multiplasmon absorption in graphene. *Phys. Rev. Lett.* **2015**, *114*, 236801.

(18) Cox, J. D.; Marini, A.; García de Abajo, F. J. Plasmon-assisted high-harmonic generation in graphene. *Nature Communications* **2017**, *8*, 14380.

(19) Kundys, D.; Van Duppen, B.; Marshall, O. P.; Rodriguez, F.; Torre, I.; Tomadin, A.; Polini, M.; Grigorenko, A. N. Nonlinear light mixing by graphene plasmons. *Nano Letters* **2018**, *18*, 282–287.

(20) Cox, J. D.; García de Abajo, F. J. Nonlinear graphene nanoplasmonics. *Accounts of Chemical Research* **2019**, *52*, 2536–2547.

(21) Yamashita, S. Nonlinear optics in carbon nanotube, graphene, and related 2D materials. *APL Photonics* **2019**, *4*, 034301.

(22) You, J. W.; Lan, Z.; Panoiu, N. C. Four-wave mixing of topological edge plasmons in graphene metasurfaces. *Science Advances* **2020**, *6*, eaaz3910.

(23) Stauber, T.; Peres, N. M. R.; Guinea, F. Electronic transport in graphene: A semiclassical approach including midgap states. *Phys. Rev. B* **2007**, *76*, 205423.

(24) Kaasbjerg, K. Atomistic T-matrix theory of disordered two-dimensional materials: Bound states, spectral properties, quasiparticle scattering, and transport. *Phys. Rev. B* **2020**, *101*, 045433.

(25) Yuan, S.; De Raedt, H.; Katsnelson, M. I. Modeling electronic structure and transport properties of graphene with resonant scattering centers. *Phys. Rev. B* **2010**, *82*, 115448.

(26) Mikhailov, S. A.; Ziegler, K. Nonlinear electromagnetic response of graphene: frequency multiplication and the self-consistent-field effects. *Journal of Physics: Condensed Matter* **2008**, *20*, 384204.

(27) Mikhailov, S. A. Theory of the giant plasmon-enhanced second-harmonic generation in graphene and semiconductor two-dimensional electron systems. *Phys. Rev. B* **2011**, *84*, 045432.

(28) Glazov, M.; Ganichev, S. High frequency electric field induced nonlinear effects in graphene. *Physics Reports* **2014**, *535*, 101–138.

(29) Cox, J. D.; Silveiro, I.; García de Abajo, F. J. Quantum effects in the nonlinear response of graphene plasmons. *ACS Nano* **2016**, *10*, 1995–2003, PMID: 26718484.

(30) Hipolito, F.; Taghizadeh, A.; Pedersen, T. G. Nonlinear optical response of doped monolayer and bilayer graphene: Length gauge tight-binding model. *Phys. Rev. B* **2018**, *98*, 205420.

(31) Cox, J. D.; Yu, R.; García de Abajo, F. J. Analytical description of the nonlinear plasmonic response in nanographene. *Phys. Rev. B* **2017**, *96*, 045442.

(32) Wang, Y.; Tokman, M.; Belyanin, A. Second-order nonlinear optical response of graphene. *Phys. Rev. B* **2016**, *94*, 195442.

(33) Chen, J.; Nesterov, M. L.; Nikitin, A. Y.; Thongrattanasiri, S.; Alonso-González, P.; Slipchenko, T. M.; Speck, F.; Ostler, M.; Seyller, T.; Crassee, I. et al. Strong plasmon reflection at nanometer-size gaps in monolayer graphene on SiC. *Nano Letters* **2013**, *13*, 6210–6215, PMID: 24188400.

(34) Alonso-González, P.; Nikitin, A. Y.; Golmar, F.; Centeno, A.; Pesquera, A.; Vélez, S.; Chen, J.; Navickaite, G.; Koppens, F.; Zurutuza, A. et al. Controlling graphene plasmons with resonant metal antennas and spatial conductivity patterns. *Science* **2014**, *344*, 1369–1373.

(35) Chen, S.; Autore, M.; Li, J.; Li, P.; Alonso-Gonzalez, P.; Yang, Z.; Martin-Moreno, L.; Hillenbrand, R.; Nikitin, A. Y. Acoustic graphene plasmon nanoresonators for field-enhanced infrared molecular spectroscopy. *ACS Photonics* **2017**, *4*, 3089–3097.

(36) Nikitin, A. Y.; Guinea, F.; García-Vidal, F. J.; Martín-Moreno, L. Edge and waveguide terahertz surface plasmon modes in graphene microribbons. *Phys. Rev. B* **2011**, *84*, 161407.

(37) Nikitin, A. Y.; Guinea, F.; Garcia-Vidal, F. J.; Martin-Moreno, L. Surface plasmon enhanced absorption and suppressed transmission in periodic arrays of graphene ribbons. *Phys. Rev. B* **2012**, *85*, 081405.

(38) Smirnova, D. A.; Shadrivov, I. V.; Miroshnichenko, A. E.; Smirnov, A. I.; Kivshar, Y. S. Second-harmonic generation by a graphene nanoparticle. *Phys. Rev. B* **2014**, *90*, 035412.

(39) Yu, R.; Cox, J. D.; Saavedra, J. R. M.; García de Abajo, F. J. Analytical modeling of graphene plasmons. *ACS Photonics* **2017**, *4*, 3106–3114.

(40) Principi, A.; Vignale, G.; Carrega, M.; Polini, M. Impact of disorder on Dirac plasmon losses. *Phys. Rev. B* **2013**, *88*, 121405.

(41) Jablan, M.; Soljačić, M.; Buljan, H. Effects of screening on the optical absorption in graphene and in metallic monolayers. *Phys. Rev. B* **2014**, *89*, 085415.

(42) Sule, N.; Willis, K. J.; Hagness, S. C.; Knezevic, I. Terahertz-frequency electronic transport in graphene. *Phys. Rev. B* **2014**, *90*, 045431.

(43) Karimi, F.; Davoody, A. H.; Knezevic, I. Nonlinear optical response in graphene nanoribbons: The critical role of electron scattering. *Phys. Rev. B* **2018**, *97*, 245403.

(44) Ullah, K.; Meng, Y.; Shi, Y.; Wang, F. Harmonic generation in low-dimensional materials. *Advanced Optical Materials* **2022**, *10*, 2101860.

(45) Koppens, F. H.; Lundeberg, M. B.; Polini, M.; Low, T.; Avouris, P. In *2D Materials: Properties and Devices*; Avouris, P., Heinz, T. F., Low, T., Eds.; Cambridge University Press, 2017; pp 104–140.

(46) Majérus, B.; Butet, J.; Bernasconi, G. D.; Valapu, R. T.; Lobet, M.; Henrard, L.; Martin, O. J. F. Optical second harmonic generation from nanostructured graphene: a full wave approach. *Opt. Express* **2017**, *25*, 27015–27027.

(47) Deng, H.; Manrique, D. Z.; Chen, X.; Panoiu, N. C.; Ye, F. Quantum mechanical analysis of nonlinear optical response of interacting graphene nanoflakes. *APL Photonics* **2018**, *3*, 016102.

(48) Thongrattanasiri, S.; Manjavacas, A.; García de Abajo, F. J. Quantum finite-size effects in graphene plasmons. *ACS Nano* **2012**, *6*, 1766–1775.

(49) Aguillon, F.; Marinica, D. C.; Borisov, A. G. Plasmons in graphene nanostructures with point defects and impurities. *The Journal of Physical Chemistry C* **2021**, *125*, 21503–21510.

(50) Araujo, P. T.; Terrones, M.; Dresselhaus, M. S. Defects and impurities in graphene-like materials. *Materials Today* **2012**, *15*, 98–109.

(51) Banhart, F.; Kotakoski, J.; Krasheninnikov, A. V. Structural defects in graphene. *ACS Nano* **2011**, *5*, 26–41.

(52) Bhatt, M. D.; Kim, H.; Kim, G. Various defects in graphene: a review. *RSC Adv.* **2022**, *12*, 21520–21547.

(53) Rodrigo, L.; Pou, P.; Pérez, R. Graphene monovacancies: Electronic and mechanical properties from large scale ab initio simulations. *Carbon* **2016**, *103*, 200–208.

(54) Lusk, M. T.; Carr, L. D. Nanoengineering defect structures on graphene. *Phys. Rev. Lett.* **2008**, *100*, 175503.

(55) Pereira, V. M.; Guinea, F.; Lopes dos Santos, J. M. B.; Peres, N. M. R.; Castro Neto, A. H. Disorder induced localized states in graphene. *Phys. Rev. Lett.* **2006**, *96*, 036801.

(56) Pereira, V. M.; Lopes dos Santos, J. M. B.; Castro Neto, A. H. Modeling disorder in graphene. *Phys. Rev. B* **2008**, *77*, 115109.

(57) Kumar, S.; Pratap, S.; Kumar, V.; Mishra, R. K.; Gwag, J. S.; Chakraborty, B. Electronic, transport, magnetic, and optical properties of graphene nanoribbons and their optical sensing applications: A comprehensive review. *Luminescence* **2022**, *n/a*.

(58) Aguillon, F.; Marinica, D. C.; Borisov, A. G. Atomic-scale control of plasmon modes in graphene nanoribbons. *Phys. Rev. B* **2022**, *105*, L081401.

(59) Kosik, M.; Müller, M. M.; Słowik, K.; Bryant, G.; Ayuela, A.; Rockstuhl, C.; Pelc, M. Revising quantum optical phenomena in adatoms coupled to graphene nanoantennas. *Nanophotonics* **2022**, *11*, 3281–3298.

(60) Leforestier, C.; Bisseling, R.; Cerjan, C.; Feit, M.; Friesner, R.; Guldberg, A.; Hammerich, A.; Jolicard, G.; Karrlein, W.; Meyer, H.-D. et al. A comparison of different

propagation schemes for the time dependent Schrödinger equation. *Journal of Computational Physics* **1991**, *94*, 59–80.

(61) Lindblad, G. On the generators of quantum dynamical semigroups. *Communications in Mathematical Physics* **1976**, *48*, 119–130.

(62) Gorini, V.; Kossakowski, A.; Sudarshan, E. C. G. Completely positive dynamical semigroups of N-level systems. *Journal of Mathematical Physics* **1976**, *17*, 821–825.

(63) Am-Shallem, M.; Levy, A.; Schaefer, I.; Kosloff, R. Three approaches for representing Lindblad dynamics by a matrix-vector notation. 2015; `https://arxiv.org/abs/1510.08634`.

(64) Kosloff, R. Quantum thermodynamics and open-systems modeling. *The Journal of Chemical Physics* **2019**, *150*, 204105.

(65) Karimi, F.; Knezevic, I. Plasmons in graphene nanoribbons. *Phys. Rev. B* **2017**, *96*, 125417.

(66) Novko, D. Dopant induced plasmon decay in graphene. *Nano Letters* **2017**, *17*, 6991–6996, PMID: 28972379.

(67) Kotov, V. N.; Uchoa, B.; Pereira, V. M.; Guinea, F.; Castro Neto, A. H. Electron-electron interactions in graphene: current status and perspectives. *Rev. Mod. Phys.* **2012**, *84*, 1067–1125.

(68) Yan, H.; Low, T.; Zhu, W.; Wu, Y.; Freitag, M.; Li, X.; Guinea, F.; Avouris, P.; Xia, F. Damping pathways of mid infrared plasmons in graphene nanostructures. *Nature Photonics* **2013**, *7*, 394–399.

(69) Langer, T.; Baringhaus, J.; Pfnür, H.; Schumacher, H. W.; Tegenkamp, C. Plasmon damping below the Landau regime the role of defects in epitaxial graphene. *New Journal of Physics* **2010**, *12*, 033017.

(70) Viola, G.; Wenger, T.; Kinaret, J.; Fogelström, M. Graphene plasmons: Impurities and nonlocal effects. *Phys. Rev. B* **2018**, *97*, 085429.

(71) Dean, J. J.; van Driel, H. M. Second harmonic generation from graphene and graphitic films. *Applied Physics Letters* **2009**, *95*, 261910.

(72) Dean, J. J.; van Driel, H. M. Graphene and few-layer graphite probed by second-harmonic generation: Theory and experiment. *Phys. Rev. B* **2010**, *82*, 125411.

(73) Kotakoski, J.; Meyer, J. C.; Kurasch, S.; Santos-Cottin, D.; Kaiser, U.; Krasheninnikov, A. V. Stone-Wales-type transformations in carbon nanostructures driven by electron irradiation. *Phys. Rev. B* **2011**, *83*, 245420.

(74) Zobelli, A.; Ivanovskaya, V.; Wagner, P.; Suarez-Martinez, I.; Yaya, A.; Ewels, C. P. A comparative study of density functional and density functional tight binding calculations of defects in graphene. *physica status solidi (b)* **2012**, *249*, 276–282.

(75) Panchakarla, L. S.; Subrahmanyam, K. S.; Saha, S. K.; Govindaraj, A.; Krishnamurthy, H. R.; Waghmare, U. V.; Rao, C. N. R. Synthesis, structure, and properties of Boron- and Nitrogen-doped graphene. *Advanced Materials* **2009**, *21*, 4726–4730.

(76) Li, Y.; Rao, Y.; Mak, K. F.; You, Y.; Wang, S.; Dean, C. R.; Heinz, T. F. Probing symmetry properties of few-layer MoS2 and h-BN by optical second-harmonic generation. *Nano Letters* **2013**, *13*, 3329–3333.

(77) An, Y. Q.; Rowe, J. E.; Dougherty, D. B.; Lee, J. U.; Diebold, A. C. Optical second-harmonic generation induced by electric current in graphene on Si and SiC substrates. *Phys. Rev. B* **2014**, *89*, 115310.

(78) Brun, S. J.; Pedersen, T. G. Intense and tunable second-harmonic generation in biased bilayer graphene. *Phys. Rev. B* **2015**, *91*, 205405.

(79) Zhang, Y.; Huang, D.; Shan, Y.; Jiang, T.; Zhang, Z.; Liu, K.; Shi, L.; Cheng, J.; Sipe, J. E.; Liu, W.-T. et al. Doping-induced second-harmonic generation in centrosymmetric graphene from quadrupole response. *Phys. Rev. Lett.* **2019**, *122*, 047401.

(80) Lobet, M.; Sarrazin, M.; Cecchet, F.; Reckinger, N.; Vlad, A.; Colomer, J.-F.; Lis, D. Probing Graphene $\chi^{(2)}$(Using a Gold Photon Sieve. *Nano Letters* **2016**, *16*, 48–54.

(81) Zhou, R.; Guo, T.; Huang, L.; Ullah, K. Engineering the harmonic generation in graphene. *Materials Today Physics* **2022**, *23*, 100649.

(82) Zhou, X.; Cheng, J.; Zhou, Y.; Cao, T.; Hong, H.; Liao, Z.; Wu, S.; Peng, H.; Liu, K.; Yu, D. Strong second-harmonic generation in atomic layered GaSe. *Journal of the American Chemical Society* **2015**, *137*, 7994–7997.

(83) Janisch, C.; Wang, Y.; Ma, D.; Mehta, N.; Elías, A. L.; Perea-López, N.; Terrones, M.; Crespi, V.; Liu, Z. Extraordinary second harmonic generation in tungsten disulfide monolayers. *Scientific Reports* **2014**, *4*, 5530.

(84) Janisch, C.; Wang, Y.; Ma, D.; Mehta, N.; Elías, A. L.; Perea-López, N.; Terrones, M.; Crespi, V.; Liu, Z. Extraordinary second harmonic generation in tungsten disulfide monolayers. *Scientific Reports* **2014**, *4*, 5530.